Article

Chain-Length-Dependent Helical Motifs and Self-Association of β-Peptides with Constrained Side Chains

Anasztzia Hetnyi, Istvn M. Mndity, Tams A. Martinek, Gbor K. Tth, and Ferenc Flp

J. Am. Chem. Soc., **2005**, 127 (2), 547-553• DOI: 10.1021/ja0475095 • Publication Date (Web): 10 December 2004

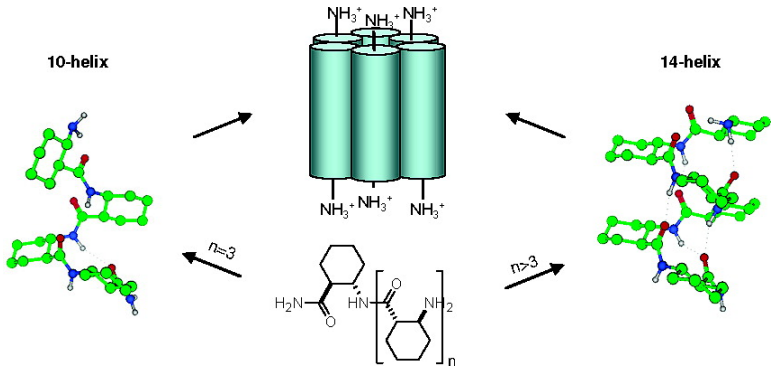

More About This Article

Additional resources and features associated with this article are available within the HTML version:

- Supporting Information
- Links to the 4 articles that cite this article, as of the time of this article download
- Access to high resolution figures
- Links to articles and content related to this article
- Copyright permission to reproduce figures and/or text from this article

View the Full Text HTML

J|A|C|S
ARTICLES
Published on Web 12/10/2004

Chain-Length-Dependent Helical Motifs and Self-Association of β-Peptides with Constrained Side Chains

Anasztázia Hetényi,[†] István M. Mándity,[†] Tamás A. Martinek,[†] Gábor K. Tóth,[‡] and Ferenc Fülöp*,[†]

Contribution from the Institute of Pharmaceutical Chemistry and Department of Medical Chemistry, University of Szeged, P.O. Box 121, H-6701 Szeged, Hungary

Received April 29, 2004; E-mail: fulop@pharma.szote.u-szeged.hu

Abstract: Homo-oligomers constructed by using *trans*-2-aminocyclohexanecarboxylic acid monomers without protecting groups were studied. Both ab initio theory and NMR measurements showed that the tetramer tends to adopt a 10-helix motif, while the pentamer and hexamer form the known 14-helix. It was concluded that the conformationally constrained backbone is flexible enough to afford both 10-helical and 14-helical motifs, this observation in turn providing evidence of the true folding process. Self-association of the helical units was also detected, and the results of variable-temperature diffusion NMR measurements strongly suggested the presence of helical bundles in methanol solution.

Introduction

The artificial secondary structures of β-peptides are of major importance in the field of self-organizing systems by virtue of the wide range of their potential applications, due to their propensity to adopt side-chain-controllable compact ordered conformations.[1−6] The conformationally constrained β-peptide oligomers containing cyclic side chains are among the most thoroughly studied models in foldamer chemistry. Homo-oligomers constructed by using *trans*-2-aminocyclohexanecarboxylic acid (*trans*-ACHC) monomers, which have protecting groups at both ends, **1**−**5** (Chart 1), are known to form a highly stable 14-helix in various solvents (methanol or pyridine).[7−15]

This structural motif is so stable that it is always predominant when the chain is longer than three monomers. The chain-length independence of the folding pattern raises the still open question of whether these oligomers exhibit a real folding process, or whether the conformational space of the monomers is too preorganized to allow partly folded or other stable secondary structures. The torsional angles φ, θ, and ψ of the β-residues extracted from the literature data[1,5,16−18] for the 10- and 14-helices with the same helicity occupy adjacent positions in the Ramachandran plot, which allows a smooth rearrangement between the two conformational states without unfolding of the helical pattern if the 10-helix is energetically available under the corresponding conditions. Accordingly, by utilizing circular dichroism (CD) spectra together with molecular dynamics simulation, Seebach et al. proposed an equilibrium between the 10- and 14-helices in β-hexapeptide derivatives with simple proteinogenic side chains[19] while Fleet et al. demonstrated experimentally that an oxetane-based β-residue leads directly to the 10-helix formation.[20] Such a conformational polymorphism is an important feature of any folded system that is

Chart 1

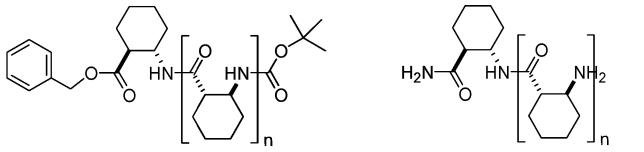

1, n = 0; **2**, n = 1; **3**, n = 2; **4**, n = 3; **5**, n = 5; **6**, n = 2; **7**, n = 3; **8**, n = 4; **9**, n = 5

[†] Institute of Pharmaceutical Chemistry.
[‡] Department of Medical Chemistry.

(1) Hill, D. J.; Mio, M. J.; Prince, R. B.; Hughes, T. S.; Moore, J. S. *Chem. Rev.* **2001**, *101*, 3893−4011.
(2) Martinek, T. A.; Fülöp, F. *Eur. J. Biochem.* **2003**, *270*, 3657−3666.
(3) Venkatraman, J.; Shankaramma, S. C.; Balaram, P. *Chem. Rev.* **2001**, *101*, 3131−3152.
(4) Saven, J. G. *Chem. Rev.* **2001**, *101*, 3113−3130.
(5) Seebach, D.; Abele, S.; Gademann, K.; Guchard, G.; Hintermann, T.; Jaun, B.; Matthews, J. L.; Schreiber, J. V. *Helv. Chim. Acta* **1998**, *81*, 932−982.
(6) (a) Epand, R. F.; Raguse, T. L.; Gellman, S. H.; Epand, R. M. *Biochemistry* **2004**, *43*, 9527−9535. (b) Schmitt, M. A.; Weisblum, B.; Gellman, S. H. *J. Am. Chem. Soc.* **2004**, *126*, 6848−6849.
(7) Appella, D. H.; Christianson, L. A.; Karle, I. L.; Powell, D. R.; Gellman, S. H. *J. Am. Chem. Soc.* **1996**, *118*, 13071−13072.
(8) Appella, D. H.; Christianson, L. A.; Karle, I. L.; Powell, D. R.; Gellman, S. H. *J. Am. Chem. Soc.* **1999**, *121*, 6206−6212.
(9) Appella, D. H.; Christianson, L. A.; Klein, D. A.; Richards, M. R.; Powell, D. R.; Gellman, S. H. *J. Am. Chem. Soc.* **1999**, *121*, 7574−7581.
(10) Barchi, J. J., Jr.; Huang, X.; Appella, D. H.; Christianson, L. A.; Durrell, S. R.; Gellman, S. H. *J. Am. Chem. Soc.* **2000**, *122*, 2711−2718.
(11) Appella, D. H.; Christianson, L. A.; Klein, D. A.; Powell, D. R.; Huang, X.; Barchi, J. J.; Gellman, S. H. *Nature* **1997**, *387*, 381−384.
(12) Gellman, S. H. *Acc. Chem. Res.* **1998**, *31*, 173−180.
(13) Appella, D. H.; Barchi, J. J.; Durell, S. R.; Gellman, S. H. *J. Am. Chem. Soc.* **1999**, *121*, 2309−2310.
(14) Raguse, T. L.; Lai, J. R.; LePlae, P. R.; Gellman, S. H. *Org. Lett.* **2001**, *3*, 3963−3966.
(15) Martinek, T. A.; Tóth, G. K.; Vass, E.; Hollósi, M.; Fülöp, F. *Angew. Chem., Int. Ed.* **2002**, *41*, 1718−1721.
(16) Banerjee, A.; Balaram, P. *Curr. Sci. India* **1997**, *73*, 1067−1077.
(17) Seebach, D.; Gademann, K.; Schreiber, J. V.; Matthews, J. L.; Hintermann, T.; Jaun, B.; Oberer, L.; Hommel, U.; Widmer, H. *Helv. Chim. Acta* **1997**, *80*, 2033−2038.
(18) Günther, R.; Hofmann, H. J. *Helv. Chim. Acta* **2002**, *85*, 2149−2168.
(19) (a) Seebach, D.; Schreiber, V. J.; Abele, S.; Daura, X.; Gunsteren, F. W. *Helv. Chim. Acta* **2000**, *83*, 34−57. (b) Daura, X.; Bakowies, D.; Seebach, D.; Fleischhauer, J.; van Gunsteren, W. F.; Krüger, P. *Eur. Biophys. J.* **2003**, *32*, 661−670.
(20) Claridge, D. W. T.; Goodman, M. J.; Moreno, A.; Angus, D.; Barker, F. S.; Taillefumier, C.; Watterson, P. M.; Fleet, W. J. G. *Tetrahedron Lett.* **2001**, *42*, 4251−4255.

designed to have a complex dynamic function in general; it is also observed for the natural α-peptides: the interplay between the α-helix and the 3_{10}-helix motif can be a crucial factor during the folding process.[21] To reveal similar intrinsic properties of the *β*-peptides and experimentally capture the conformational polymorphism in high-resolution solution structures, short oligomers with conformationally constrained side chains without terminal protecting groups were studied in the present work. We set out to discover the limits of the flexibility of *trans*-ACHC oligomers and to test the ability of these oligomers to adopt the 10-helix motif besides the well-known 14-helix, which would suggest that the 10-helix may be a potential conformational intermediate in the folding process toward the thermodynamically stable 14-helix.

Results and Discussion

In our approach, the potential energy hypersurfaces of *trans*-ACHC homo-oligomers without protecting groups, **6**−**9** (Chart 1), were probed first by a standard restrained simulated annealing conformational search protocol, carried out by using molecular mechanics and distance restraints between the relevant H-bond pillar atoms. The resulting most stable structures for **7**−**9** were optimized without restraints for both the 10- and 14-helices. Final minimizations were carried out by using an ab initio quantum mechanical method[22] at the RHF/3-21G level in a vacuum, as this has been reported to provide a good approximation for the geometry of the *β*-peptides.[23] The ab initio structures converged to the corresponding local minimum of the potential energy surface. To take into account the effects of more diffuse basis sets and the electron correlation, the energies were calculated at the B3LYP/6-311G** level too (Figure 1). The conformational energy differences between the 10- and 14-helices ($\Delta E = E_{10} - E_{14}$) proved to be rather low in terms of the nonbonding interaction energy scale, indicating a possible energetic availability of the 10-helix. The ΔE values clearly reveal a trend of an increasing relative stability for the 10-helix motif as the chain length decreases. The energy difference obtained with the different approximation levels for **7** predict a conformational equilibrium between the 10- and 14-helices, with a slight preference for the 10-helix in the case of the RHF/3-21G level. These findings presage the tendency for the unprotected tetramer to adopt the 10-helical motif, which is surprising in light of the earlier literature results on similar constrained *β*-peptides with protecting groups and offers a possibility for experimental testing.

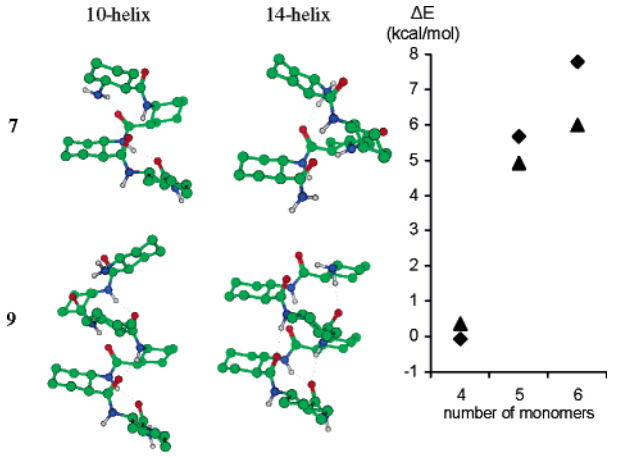

Figure 1. Some of the resulting ab initio structures, and the chain-length dependence of the conformational energy difference between the 10- and 14-helices: ◆, RHF/3-21G; ▲, B3LYP/6-311G**.

The Boc-(1*S*,2*S*)-ACHC monomer was synthesized by a literature method.[24] The chain assembly was carried out in the solid phase; after the third amino acid, the acyl fluoride method[25−27] was used, due to the difficulty of elongation of the peptide chain. The peptides were detached from the resin by using liquid HF, and the product was isolated by RP-HPLC. Products were characterized by means of various NMR methods, including COSY, TOCSY, and ROESY, in 8 mM CD_3OD and DMSO solutions.

For assessment of the conformational stability of the peptides in CD_3OD, $^1H-^2D$ amide proton exchange was utilized. For **6**, an unfolded conformation was found, as deciphered from the immediate amide proton exchange. Following the dissolution of **7**, ^1H NMR indicated that the amide protons exchanged completely only in 2 weeks. The amide protons in **8** and **9** still showed strong resonances after the same period of time. The shielded amide protons of the residues in the corresponding oligomers were assigned (Figure 2).

The observations confirmed that the studied oligomers adopt very stable intramolecular H-bonded folding patterns in CD_3OD solution. As concerns the previously reported *trans*-ACHC oligomers with protecting groups, the amide proton signals were lost within 65 h,[7] which may suggest considerably more shielded NH protons in our models, but a direct comparison must be made with caution because of the incidentally different concentrations of residual acid (TFA) stemming from the chromatographic separation and sample preparation protocol. The $^1H-^2D$ amide proton exchange experiments were therefore repeated for **9** with an elevated TFA concentration of 1.0% v/v. The residual signals of the most shielded protons exhibit a relative intensity of 0.2 after 65 h for **9** (Figure 3). The usual TFA concentration during HPLC separations is 0.1% v/v; hence, the applied TFA level in these $^1H-^2D$ exchange experiments is drastically higher than one would expect in a normal setup. Accordingly, these results still support the view of highly shielded and stable H-bonds in the studied compounds.

(21) Bolin, A. K.; Millhauser, L. G. *Acc. Chem. Res.* **1999**, *32*, 1027−1033.
(22) Frisch, M. J.; Trucks, G. W.; Schlegel, H. B.; Scuseria, G. E.; Robb, M. A.; Cheeseman, J. R.; Montgomery, J. A., Jr.; Vreven, T.; Kudin, K. N.; Burant, J. C.; Millam, J. M.; Iyengar, S. S.; Tomasi, J.; Barone, V.; Mennucci, B.; Cossi, M.; Scalmani, G.; Rega, N.; Petersson, G. A.; Nakatsuji, H.; Hada, M.; Ehara, M.; Toyota, K.; Fukuda, R.; Hasegawa, J.; Ishida, M.; Nakajima, T.; Honda, Y.; Kitao, O.; Nakai, H.; Klene, M.; Li, X.; Knox, J. E.; Hratchian, H. P.; Cross, J. B.; Adamo, C.; Jaramillo, J.; Gomperts, R.; Stratmann, R. E.; Yazyev, O.; Austin, A. J.; Cammi, R.; Pomelli, C.; Ochterski, J. W.; Ayala, P. Y.; Morokuma, K.; Voth, G. A.; Salvador, P.; Dannenberg, J. J.; Zakrzewski, V. G.; Dapprich, S.; Daniels, A. D.; Strain, M. C.; Farkas, O.; Malick, D. K.; Rabuck, A. D.; Raghavachari, K.; Foresman, J. B.; Ortiz, J. V.; Cui, Q.; Baboul, A. G.; Clifford, S.; Cioslowski, J.; Stefanov, B. B.; Liu, G.; Liashenko, A.; Piskorz, P.; Komaromi, I.; Martin, R. L.; Fox, D. J.; Keith, T.; Al-Laham, M. A.; Peng, C. Y.; Nanayakkara, A.; Challacombe, M.; Gill, P. M. W.; Johnson, B.; Chen, W.; Wong, M. W.; Gonzalez, C.; Pople, J. A. *Gaussian 03*, Revision A.1; Gaussian, Inc.: Pittsburgh, PA, 2003; http://www.gaussian-.com.
(23) (a) Beke, T.; Csizmadia, I. G.; Perczel, A. *J. Comput. Chem.* **2004**, *25*, 285−307. (b) Mohle, K.; Gunther, R.; Thormann, M.; Sewald, N.; Hofmann, H. J. *Biopolymers* **1999**, *50*, 167−184.
(24) Kanerva, L. T.; Csomós, P.; Sundholm, O.; Bernáth, G.; Fülöp, F. *Tetrahedron: Asymmetry* **1996**, *7*, 1705−1716.
(25) Carpino, L. A.; Elfaham, A. *J. Am. Chem. Soc.* **1995**, *117*, 5401−5402.
(26) Wenschuh, H.; Beyermann, M.; Winter, R.; Bienert, M.; Ionescu, D.; Carpino, L. A. *Tetrahedron Lett.* **1996**, *37*, 5483−5486.
(27) Carpino, L. A.; Beyermann, M.; Wenschuh, H.; Bienert, M. *Acc. Chem. Res.* **1996**, *29*, 268−274.

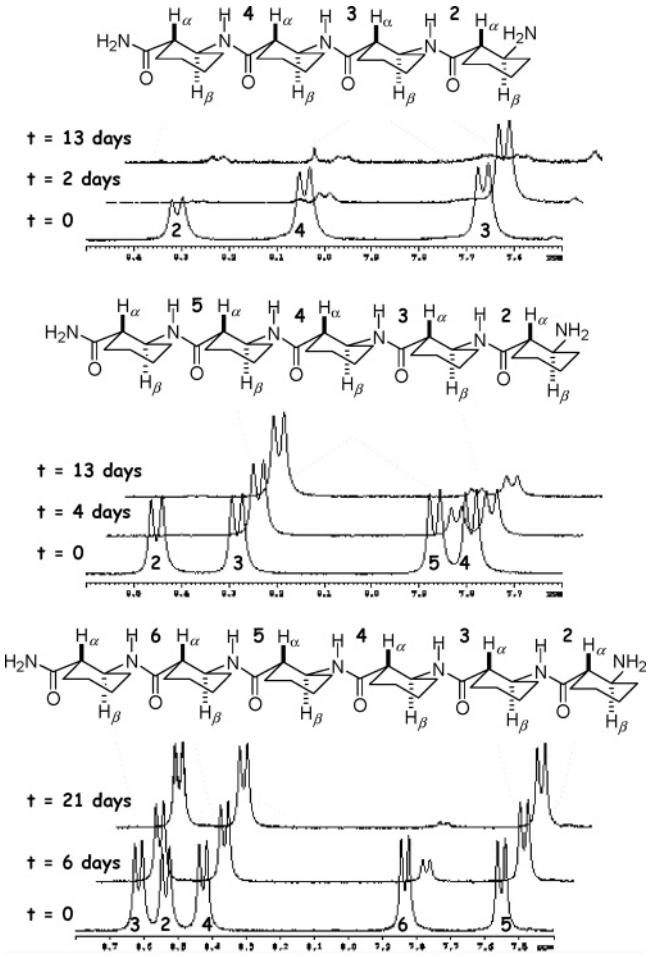

Figure 2. NH/HD exchange results for **7**−**9** in CD_3OD.

The high-resolution 3D structure assignment was carried out by running ROESY spectra with 225 ms (Figure 4) and 400 ms spin lock in CD_3OD. The intensity ratio (R) of the cross-peaks $NH_i-C^{\alpha}H_{i-1}$ and $NH_i-C^{\beta}H_i$ calculated according to eq 1, where I_{NOE} designates the integrated and offset-compensated

$$R = I_{NOE}(NH_i-C^{\alpha}H_{i-1})/I_{NOE}(NH_i-C^{\beta}H_i) \qquad (1)$$

ROESY cross-peak intensities, is a sensitive indicator of the overall fold of the oligomers because it is dependent on the sixth power of the relative distances.[15] By using secondary structure motifs of (1*S*,2*S*)-ACHC obtained by molecular modeling, representative R values are estimated as 3.51, 5.83, and 5.61 for the right-handed 12-helix, left-handed 10-helix, and left-handed 14-helix, respectively. The random coil gives an R value of 2.1. It is clear that the 10- and 14-helices cannot be distinguished in this way, considering their similar R values and the usual experimental error; nevertheless, the overall fold can be determined.

Comparison of the experimental intensity ratios and the theoretical values reveals good agreement with the left-handed 10- or 14-helical fold for each compound, with the exception of the N-terminal residues (Table 1). For **7**, the $NH_2-C^{\alpha}H_1$ NOE interaction is missing (i.e., $R = 0$, Figure S6 in the Supporting Information), which is a major deviation from the regular helix structure, pointing to a fraying or unusually oriented N-terminal residue. This observation is supported by the relatively faster exchange rate of NH_2 and the considerable upfield shift of $C^{\alpha}H_1$

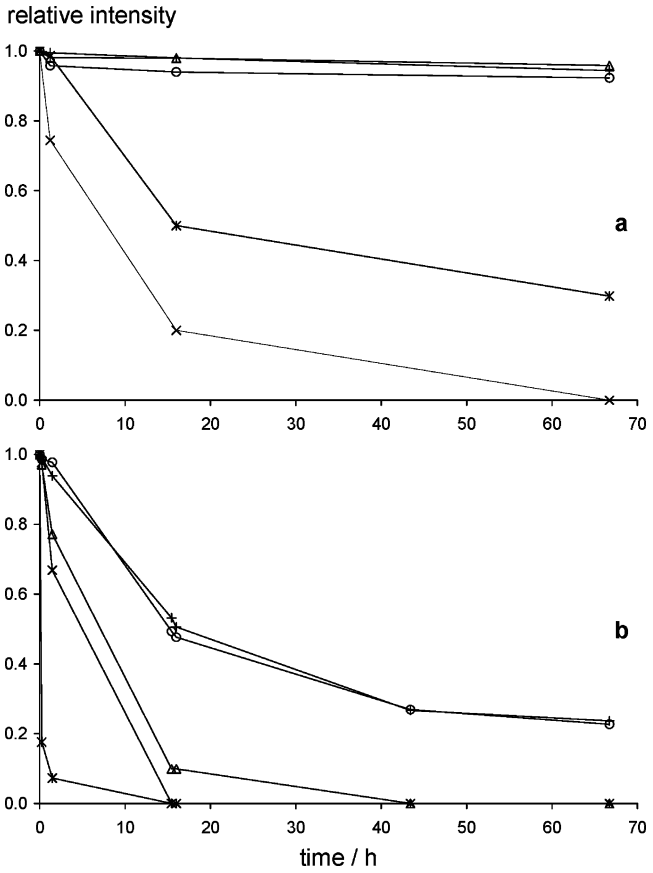

Figure 3. Comparison of the NH/ND exchange rates: (a) without additional TFA; (b) with 1% TFA. The displayed intensities are assigned as follows: ×, NH_2; ○, NH_3; +, NH_4; △, NH_5; ∗, NH_6.

(2.14 ppm) in comparison with those for **8** (2.96 ppm) and **9** (2.95 ppm). For **8** and **9**, the R values involving the first residue are slightly decreased, but there is not a dramatic difference. The antiperiplanar arrangement of the $NH_i-C^{\beta}H_i$ protons in both the 10- and 14-helices was confirmed by the uniform $^3J(NH_i-C^{\beta}H_i)$ values of ca. 9 Hz.

As regards the theoretical models, another major difference between the two helical structures is that the 10-helix should give $C^{\alpha}H_i-C^{\beta}H_{i+2}$ and the 14-helix $C^{\alpha}H_i-C^{\beta}H_{i+3}$ NOE interactions. For **7**, a marked signal can be observed between the protons at 2.85 ppm, unambiguously assigned to $C^{\alpha}H_2$, and at 4.02 ppm. The resonances of $C^{\beta}H_2$ and $C^{\beta}H_4$ overlap near 4.02 ppm, but analysis of the vicinal coupling constant pattern clearly demonstrates the prevailing *trans*-diaxial orientation of $C^{\beta}H_2$ and $C^{\alpha}H_2$, which rules out their proximity of <2.5 Å, estimated from the cross-peak intensity. The nonoverlapping intraresidue $C^{\beta}H_i-C^{\alpha}H_i$ NOE signals for residues 3 and 4 are of much lower intensities (25%). The cross-peak in question is therefore assigned to the long-range $C^{\alpha}H_2-C^{\beta}H_4$ interaction. The $C^{\alpha}H_1-C^{\beta}H_3$ interaction in the ROESY spectrum at the given signal-to-noise ratio is indistinct, in parallel with the irregular N-terminal residue orientation deciphered from the missing $NH_2-C^{\alpha}H_1$ NOE cross-peak. The proximity of $C^{\alpha}H_2-C^{\beta}H_4$ can only be maintained by the cooperation of two H-bonds, CO_4-NH_3 and CO_3-NH_2, forming a stable 10-helix motif involving residues 2−4, while the absence of the $C^{\alpha}H_1-C^{\beta}H_3$ and $NH_2-C^{\alpha}H_1$ NOE interactions can be explained by an irregularly oriented N-terminal residue. The rotation of the first residue is not hindered sterically or by hydrophobic stabilization in the

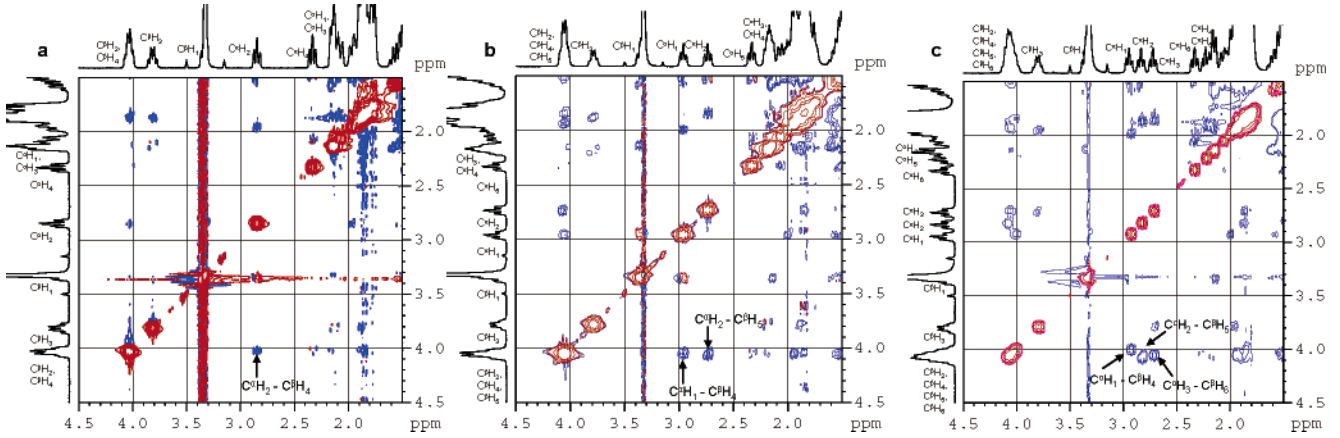

Figure 4. Diagnostic cross-peaks in ROESY spectra and signal assignments for (a) **7**, (b) **8**, and (c) **9** in CD_3OD: red, positive intensity levels; blue, negative intensity levels.

Table 1. *R* Values from ab Initio Structures and NMR Measurements

	9			8			7		
i	calcd 10-helix	calcd 14 -helix	exptl	calcd 10-helix	calcd 14-helix	exptl	calcd 10-helix	calcd 14-helix	exptl
2	6.1	4.9	3.8	5.3	6.1	3.7	5.8	6.3	0.0
3	7.1	4.9	5.9	5.2	6.3	4.6	5.5	4.4	4.2
4	6.6	4.7	5.7	6.0	6.1	4.8	6.0	6.5	4.2
5	5.7	5.7	6.0	4.8	6.3	6.0			
6	5.9	5.1	7.5						

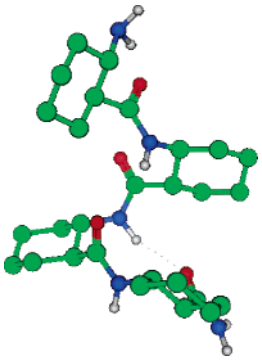

Figure 5. Prevailing structure of **7** determined by NMR.

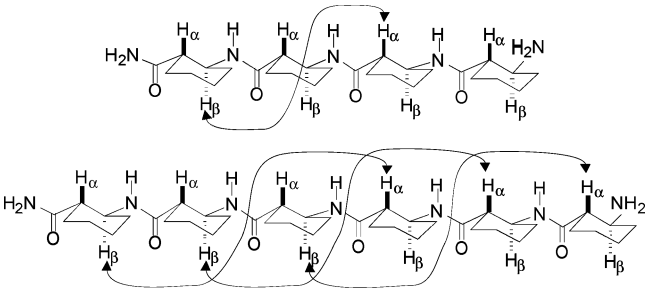

Figure 6. NOE cross-peaks defining long-range $C^\alpha H_2 - C^\beta H_4$ interaction for **7** and $C^\alpha H_i - C^\beta H_{i+3}$ interactions for **9**.

10-helix due to the lack of $i-(i+3)$ side-chain−side-chain proximity (Figure 5). The preference for the distorted 10-helix motif in **7** can be explained by the fact that only three amide bonds are available for H-bonding stabilization. In the 10-helix conformation, two H-bonds can be formed for such a short chain length, while the 14-helix facilitates only one H-bond. The extra electrostatic stabilization counteracts the conformational strain encountered at the monomer level.[2] In contrast with the ACHC tetramer with an unprotected N-terminal, the ACHC tetramer studied by Gellman et al.[8,10] possesses four amide groups. The additional amide NH on the first residue can also participate in a H-bond, furnishing two stabilizing H-bonds in the 14-helix, and here the contribution from the third H-bond cannot counteract the conformational strain occurring when the N-terminal residue is also regularly positioned in the 10-helix. These findings suggest that the formation of a stable 14-helix requires at least four amide bonds in the β-peptide chain and the helix nucleation with three residues can start with the 10-helix motif.

For **8** and **9**, all the $C^\alpha H_i - C^\beta H_{i+3}$ interactions could be readily identified (Figure 6). These results strongly suggest that **8** and **9** adopt a left-handed 14-helix pattern, which is in accord with the earlier literature results and proves that removal of the protecting groups does not affect the stability of the 14-helix at this chain length. The lower *R* values found for the first residues support a fraying N-terminal, but the presence of the $C^\alpha H_1 - C^\beta H_4$ NOE interaction is promoted by the sterically hindered rotation caused by the well-known $i-(i+3)$ side-chain−side-chain interaction in the 14-helix.

The presence of the H-bonds stabilizing the helices was tested by using IR spectroscopy in the intramolecular H-bond-promoting solvent CD_3OH at a concentration of 8 mM (Figure 7). The carbonyl stretching vibrations of the peptide backbone are sensitive markers of the peptide secondary structure, as the vibrational frequency of each C═O bond depends on the H-bonding and the interactions between the amide units, both of which are influenced by the secondary structure. For all the molecules, two characteristic bands were observed, at 1679 and 1648 cm^{-1}. The high-frequency band was assigned to amide CO groups not involved as acceptors in H-bonding, and the low-frequency band to intramolecular H-bonds. The relative intensity of the 1648 cm^{-1} band increases on going from **7** to **9**, which is in line with the assigned secondary structures. In

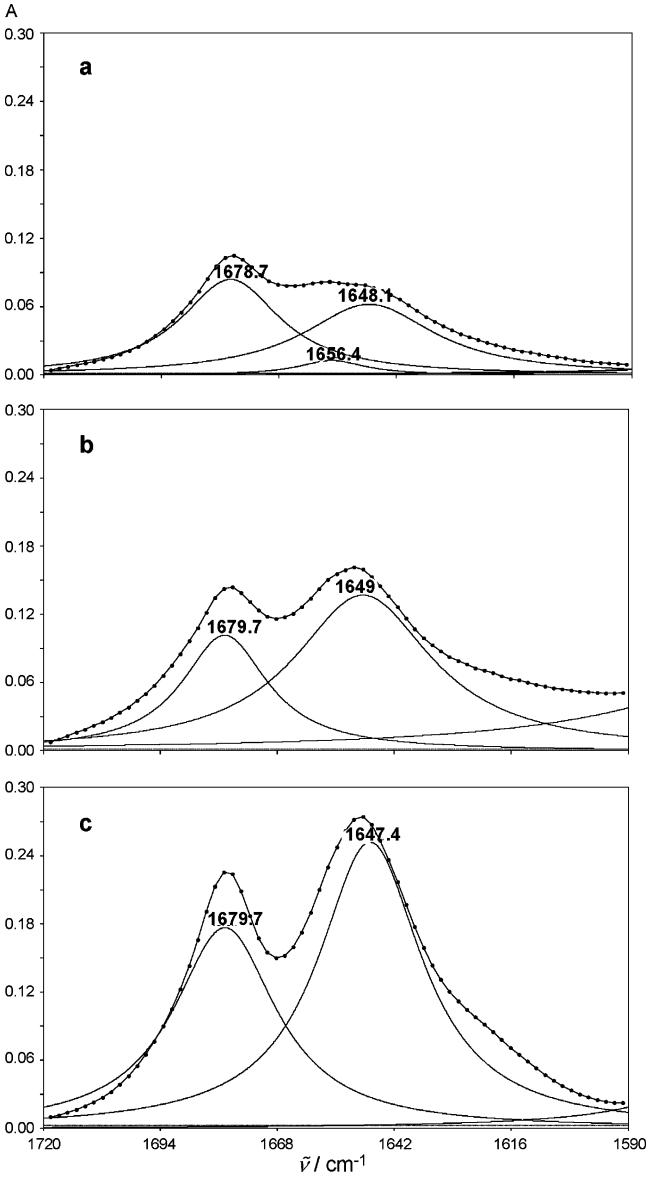

Figure 7. Comparison of the IR spectra of *trans*-ACHC oligomers recorded in CD_3OH: (a) **7**, (b) **8**, and (c) **9**. The thick curve denotes the measured data, and the thin curves denote the component bands obtained from nonlinear fitting.

the amide I region for **7**, a weak shoulder was observed at 1656 cm^{-1}, which may be indicative of a weaker H-bond. This observation can be correlated with the fraying N-terminal of the tetramer and may provide additional evidence of the structural dissimilarity of **7**.

A series of publications have revealed that the interpretation of the CD spectra of β-peptides requires special care, as they are extremely sensitive to minor variations in the structure that do not affect the overall fold of the molecule.[8,19] The best assignment between the CD features and the 10- and 14-helical patterns appears to be as follows: (i) the 10-helix motif gives rise to a single strong Cotton effect near 205 nm and (ii) the 14-helix motif contributes with Cotton effects of opposite sign near 200 nm and near 215 nm.[19a] We compared the CD spectra for the model compounds (Figure 8).

The data obtained for **7**−**9** display similar features, a positive Cotton effect at 197 nm and a negative Cotton effect at 217 nm, but there are marked differences in the relative intensities

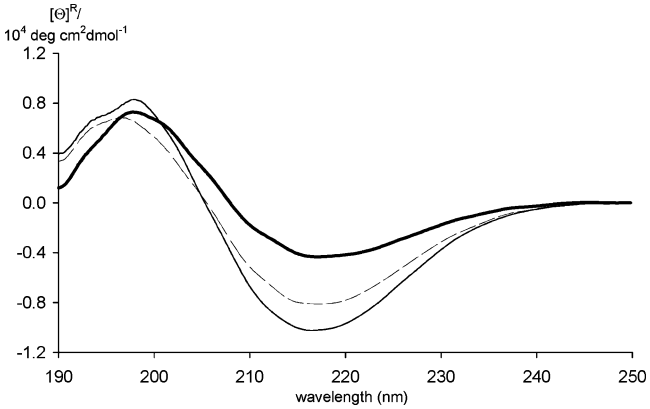

Figure 8. Comparison of the CD spectra of *trans*-ACHC oligomers recorded in CD_3OH: thick curve, **7**; dashed curve, **8**; thin curve: **9**. The mean residue ellipticity is depicted.

of the Cotton effects for **7** as compared with the longer oligomers. The intensity of the negative Cotton effect at around 217 nm is significantly less for **7**, while the positive Cotton effect, at slightly lower frequency, gives a signal comparable in strength with those for **8** and **9**. The assignment rule of Seebach et al.[19] allows the considerably lower signal near 217 nm and the strong positive Cotton effect for **7** to be assigned to a conformational ensemble containing the 10-helix motif in significant amount or possibly as the predominant conformation in light of the NMR results. The clear unbiased Cotton effects with opposite sign for **8** and **9** can be assigned to the 14-helix.

The intriguing question of the much higher shielding from the solvent for the NH protons may be explained by the self-association phenomenon on the basis of the early works of Gellman et al.[8,14] For characterization of the self-association, diffusion NMR measurements with a stimulated gradient echo and longitudinal eddy current delay were used.[28] Through exploitation of the relationship between the apparent hydrodynamic radius and the diffusion constant, the aggregation numbers (N) were determined by following the literature methods,[28,29] via the following equations:

$$N = \frac{(m_{TMS}/m)^3 V_{TMS}}{V_i} \quad (2)$$

$$m = -\frac{\ln(I/I_0)}{k} \quad (3)$$

$$k = (\gamma G \delta)^2 (\Delta - \delta/3) \quad (4)$$

where I is the corresponding NMR signal intensity, G is the gradient strength, V is the molecular volume, γ is the gyromagnetic ratio, and Δ and δ are the diffusion delay and gradient pulse length parameters for the stimulated gradient echo pulse sequence. The aggregation numbers were determined from three independent measurements with an average error of 0.12 (Tables S1−S3 and Figures S3−S5 in the Supporting Information). As an internal reference, TMS was used. This measurement samples the ensemble average of the molecules; hence, the resulting aggregation number is an average over the aggregated species, giving rise to nonintegral values. The diffusion model utilized

(28) Antalek, B. *Concepts Magn. Reson.* **2002**, *14*, 225−258.
(29) Valentini, M.; Vaccaro, A.; Rehor, A.; Napoli, A.; Hubbell, J. A.; Tirelli, N. *J. Am. Chem. Soc.* **2004**, *126*, 2142−2147.

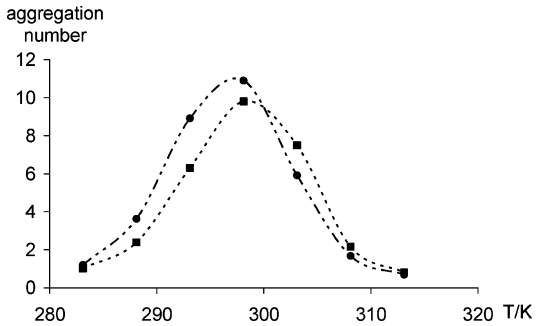

Figure 9. Temperature dependence of the aggregation numbers: ●, for **7**; ■, for **9**.

assumes spherical symmetry for the species, this condition being met for the helix monomers, where both the helix diameter and the helix length are approximately 10 Å. The aggregated species diverge from spherical symmetry, but the trends in the aggregation propensities can be followed reasonably well.

The measured aggregation numbers, 5.91, 6.60, and 7.49, revealed an increasing trend for **7**, **8**, and **9**, respectively, in CD_3OD at 303.1 K. The driving force for the aggregation may be a specific head-to-tail H-bond pattern leading to a rodlike superstructure, and/or the solvent-driven side-by-side hydrophobic interactions between the helical units, resulting in helix bundles. Head-to-tail NOE interactions were not detected, and a rodlike assembly would not explain the extra NH shielding observed in the exchange experiments; this hypothesis can therefore be eliminated. The temperature-dependent aggregation number measurements furnished a maximum curve (Figure 9), which is characteristic of ionic tensides.[30−32] For this type of molecule, a lower temperature is advantageous for the formation of a stable sovation shell, preventing aggregation, while a higher temperature affords a higher disaggregating kinetic energy. This result supports solvent-driven helix bundle formation, which can effectively increase the shielding of the NH protons from the solvent. The self-association does not affect the secondary structure stability, as constant helical patterns were observed at the disaggregating temperature of 310 K.

Conclusions

It may be concluded that the conformationally constrained backbone is flexible enough to afford both 10- and 14-helical motifs; in turn, this observation provides evidence of the true folding process, and the question arises of whether the 10-helix is a nucleating intermediate in the folding of the 14-helix. In summary, it may be stated that a sharper picture of the folding rules of conformationally constrained β-peptides was obtained. The evidence of the chain-length-dependent conformational preference indicates the flexibility of the studied models despite the conformationally constrained side chains, which could be exploited to construct folded structures with dynamic functionality. The studied models undergo hydrophobically stabilized helical bundle formation in CD_3OD, where the propensity for self-association increases with the chain length. This finding draws the attention of the β-peptide community to the fact that oligopeptide aggregation might always be present, even if the usual indicators such as NMR signal broadening cannot be observed. This points to the intrinsic self-associating propensity of helical units with hydrophobic side chains in polar solvents.

Experimental Section

Peptide Synthesis. The synthesized (*S*,*S*)-ACHC-containing oligomers were as follows: H−(ACHC)$_3$−NH$_2$ (**6**), H−(ACHC)$_4$−NH$_2$ (**7**), H−(ACHC)$_5$−NH$_2$ (**8**), and H−(ACHC)$_6$−NH$_2$ (**9**). The sequences were synthesized by a solid-phase technique, utilizing tBoc chemistry.[33] The peptide chains were elongated on a *p*-methylbenzhydrylamine resin (0.63 mmol/g), and the syntheses were carried out manually on a 1 mmol scale. Couplings were performed with 3 equiv of dicyclohexylcarbodiimide and hydroxybenzotriazole, without difficulties until the third amino acid. After this incorporation, the coupling step became extremely difficult: all the usual coupling methods, including the *O*-(benzotriazol-1-yl)-*N*,*N*,*N*′,*N*′-tetramethyluronium hexafluorophosphate or *O*-(7-azabenzotriazol-1-yl)-*N*,*N*,*N*′,*N*′-tetramethyluronium hexafluorophosphate methods failed (more than 50% of the free amino function of the third amino acid remained unacylated, even after three repeated coupling steps and an elongated reaction time). Only the acid fluoride-producing tetramethylfluoroformamidinium hexafluorophosphate coupling proved more successful; merely approximately 20% of the amino functions remained unacylated after one coupling step (by repetition, this could be decreased to 10%). The amino acid incorporation was monitored by means of the ninhydrin test[34] and by the cleavage of aliquots from the resin. The completed peptide resins were treated with liquid HF/dimethyl sulfide/*p*-cresol/*p*-thiocresol (86:6:4:2, v/v) at 0 °C for 1 h. The HF was removed, and the resulting free peptides were solubilized in 10% aqueous acetic acid, filtered, and lyophilized. The crude peptides were purified by reversed-phase HPLC (RP HPLC), using a Nucleosil C-18 7 μm column (16 × 250 mm). The HPLC apparatus was made by Knauer (Berlin, Germany). The solvent system used was as follows: 0.1% trifluoroacetic acid (TFA) in water, 0.1% TFA, 80% acetonitrile in water, gradient 0% → 0% B over 15 min, then 25% → 55% over 60 min, flow rate 3.5 mL/min, detection at 206 nm (Figure S1 in the Supporting Information). The appropriate fractions were pooled and lyophilized. The purified peptides were characterized by mass spectrometry, using a Finnigan TSQ 7000 tandem quadruple mass spectrometer equipped with an electrospray ion source (Figure S2 in the Supporting Information).

NMR Experiments. NMR measurements were performed on a Bruker Avance DRX 400 MHz spectrometer with a multinuclear probe with a *z*-gradient coil in 8 mM CD_3OD and DMSO solutions at 303.1 K. The ROESY measurements were performed with a WATERGATE water suppression scheme. For the ROESY spinlock, 225 and 400 ms mixing times were used, and the number of scans was 64. The TOCSY measurements were performed with homonuclear Hartman−Hahn transfer with the MLEV17 sequence, with an 80 ms mixing time, and the number of scans was 32. For all the 2D spectra 2K time domain points and 512 increments were applied. The processing was carried out by using a cosine-bell window function, single zero filling, and automatic baseline correction.

The PFGSE NMR measurements were performed by using the stimulated echo and longitudinal eddy current delay (LED) sequence.[28] A time of 1.5 ms was used for the dephasing/refocusing gradient pulse length (δ), and 100 ms for the diffusion delay (Δ). The gradient strength was changed quadratically from 5% to 95% of the maximum value (B-AFPA 10 A gradient amplifier), and the number of steps was 16. Each measurement was run with 32 scans and 16K time domain points. For the processing, an exponential window function and single zero filling were applied. During the diffusion measurements, the fluctuation of the temperature was less than 0.1 K. Prior to the NMR scans, all the samples were equilibrated for 30 min.

(30) González-Pérez, A.; Del Castillo, J. L.; Czapkiewicz, J.; Rodríguez, J. R. *Colloids Surf., A* **2004**, *232*, 183−189.
(31) Jolicoeur, J.; Philip, P. R. *Can. J. Chem.* **1974**, *52*, 1834.
(32) The studied β-peptides were dissolved as TFA salts.
(33) Merrifield, R. B. *J. Am. Chem. Soc.* **1963**, *85*, 2149−2154.
(34) Kaiser, E.; Colescott, R. L.; Bossinger, C. D.; Cook, P. *J. Anal. Biochem.* **1970**, *34*, 595−598.

IR Experiments. The IR measurements were performed on a Bio-Rad Digilab Division FTS 65A/869 FT-IR spectrometer. The samples were prepared as 8 mM solutions in CD_3OH. The experiments were run with the spectral window 4000−400 cm^{-1} at an optical resolution of 4 cm^{-1} with 256 scans. The detector was DTGS (deuterated tryglycyl sulfate); the sample was placed in a 0.1 mm liquid cell, and KBr windows were applied.

CD Measurements. CD spectra were measured on a Jobin-Yvon Mark VI dichrograph at 25 °C in a 0.02 cm cell. Four spectra were accumulated for each sample. The baseline spectum recorded with only the solvent was subtracted from the raw data. The concentration of the sample solutions was 4 mM in CD_3OH. Molar ellipticity, [Θ], is given in deg cm^2 $dmol^{-1}$. The data were normalized for the number of chromophores.

Molecular Mechanical Calculations. Molecular mechanical simulations were carried out on an HP workstation xw6000 in the Chemical Computing Group's Molecular Operating Environment. For the energy calculations, the MMFF94s force field was used, with a 15 Å cutoff for van der Waals and Coulomb interactions. The lowest-energy structures of the 10- and 14-helices for **7**−**9** were determined by using relevant H-bond pillar atom distance restraints: NH_i-CO_{i+1} and NH_i-CO_{i+2} for the 10-helix and 14-helix, respectively. Before the restrained simulated annealing (RSA), a random structure set of 100 molecules was generated by saving the conformations during a 100 ps dynamics simulation at 1000 K every 1000 steps. The RSA was performed for each structure with an exponential temperature profile in 75 steps, and a total duration of 25 ps, and the H-bond restraints were applied as a 10 (kcal/mol)/$Å^2$ penalty function. Minimization was applied after every RSA in a cascade manner, using the steepest descent, conjugate gradient, and truncated Newton algorithm.

Ab Initio Calculations. The molecular structure, stereochemistry, and geometry of the ACHC oligomers were exclusively defined in terms of their **z**-matrix internal coordinate system. The optimizations were carried out with the Gaussian03 program by using the RHF/3-21G basis set with a default setup. Single-point energies were additionally calculated by using density-functional theory at the B3LYP/6-311G** level.

Acknowledgment. We thank the Hungarian Research Foundation (OTKA Grant Nos. TO34912, TS04888, and F038320) for financial support.

Supporting Information Available: RP-HPLC chromatograms, MS spectra, details of the determination of aggregation numbers, signal assignments in CD_3OD and DMSO-d_6, ROESY cross-peak assignment, ^1H NMR and ROESY spectra in DMSO, and coordinates and energies of the ab initio structures. This material is available free of charge via the Internet at http://pubs.acs.org.

JA0475095